Electronic Supplementary Information (ESI) for Chemical Communications

Constructing highly active Co sites in Prussian Blue Analogues for Boosting Electrocatalytic Water Oxidation

Hanjun Zou,[†ab] Xue Liu,[†a] Kaiwen Wang,[c] Youyu Duan,[a] Cong Wang,[c] Bin Zhang,[b] Kai Zhou,[b] Danmei Yu,[d] Liyong Gan,[*a] Xiaoyuan Zhou[*ab]

[a] College of Physics and State Key Laboratory of Coal Mine Disaster Dynamics and Control, Chongqing University, Chongqing 401331, China

[b] Analytical and Testing Center, Chongqing University, Chongqing 401331, China

[c] Beijing Key Laboratory of Microstructure and Property of Advanced Materials Beijing University of Technology, Beijing 100024, China

[d] School of Chemistry and Chemical Engineering, Chongqing University, Chongqing 401331, China

[†] These authors contributed equally to this work.

*Corresponding authors at:
College of Physics and State Key Laboratory of Coal Mine Disaster Dynamics and Control, Chongqing University, Chongqing 401331, China

Analytical and Testing Center, Chongqing University, Chongqing 401331, China
E-mail address: ganly@cqu.edu.cn; xiaoyuan2013@cqu.edu.cn

Contents

Experimental section

Synthesis of CoFe-PBA nanocube: CoFe-PBA nanocube was synthesized by a co-precipitation method under ambient condition. 0.39 g of $Co(CH_3COO)_2 \cdot 4H_2O$ and 0.88 g of $C_6H_5Na_3O_7 \cdot 2H_2O$ were dissolved in 40 mL of ultrapure water to form solution A. 0.53 g of $K_3Fe(CN)_6$ was dissolved in 60 mL of ultrapure water to form solution B. Subsequently, solution B was added into solution A under magnetic stirring for 1 min and then the mixed solution was aged at room temperature for 26 h. Finally, the CoFe-PBA nanocube was obtained by centrifuging and washing the resultant suspension solution several times with ultrapure water and ethanol followed by drying at 60°C overnight.

Synthesis of CoFeZn-PBA composite structure: 0.39g of $Co(CH_3COO)_2 \cdot 4H_2O$, 0.23 g of $ZnSO_4 \cdot 7H_2O$ and 0.88 g of $C_6H_5Na_3O_7 \cdot 2H_2O$ were dissolved in 40 mL of ultrapure water to form solution C. Then, solution B was added into solution C under magnetic stirring for 1 min and the obtained solution was aged at room temperature for 26 h. Finally, CoFeZn-PBA sample (Co: Fe: Zn = 3: 3: 1.5) was obtained by centrifuging and washing the resulting suspension solution several times with ultrapure water and ethanol followed by drying at 60°C overnight. Additionally, CoFeZn-PBA samples with different Co: Fe: Zn ratios (Co: Fe: Zn = 3: 3: 1, 3: 3: 2, 3: 3: 2.5) and different co-precipitation times (20 h, 26 h, 32 h, 38 h) were also synthesized through the uniform synthetic condition as described above.

Synthesis of CoCo-PBA nanocube: 0.15 g of $Co(CH_3COO)_2 \cdot 4H_2O$ and 0.26 g of $C_6H_5Na_3O_7 \cdot 2H_2O$ were dissolved in 20 mL of ultrapure water to form solution A. 0.13 g of $K_3Co(CN)_6$ was dissolved in 20 mL of ultrapure water to form solution B. Subsequently, solution B was added into solution A under magnetic stirring for 1 min and then the mixed solution was aged at room temperature for 26 h. Finally, the CoCo-PBA nanocube was obtained by centrifuging and washing the resultant suspension solution several times with ultrapure water and ethanol followed by drying at 60°C overnight.

Material characterization: The X-ray diffraction (XRD, PANalytical X'Pert Powder) was performed using Cu-Kα radiation (λ = 1.54186 Å) at a voltage of 40 kV and a current of 40 mA in the 2θ range of 10 ~ 60° to identify the crystal phase and structure of the samples. Raman spectra were obtained at room temperature using a LabRAM HR Evolution with a 532 nm laser as the excitation source. The morphology and chemical composition of the samples were characterized by transmission electron microscope (TEM, FEI Talos F200S) and scanning electron microscope (SEM, FEI Quattro S). The X-ray photoelectron spectroscopy (XPS) spectra were collected utilizing a charge neutralizer and calibrated by the C 1*s* peak of carbon impurities at 284.8 eV. N_2 adsorption/desorption isotherms were performed using the BELSORP-max-II at 77 K to evaluate the specific surface area, pore size distribution and pore volume by Horvath-Kawazoe and t-pot method. Fourier transform infrared (FTIR) spectra were tested by Thermo Fisher Scientific Nicolet iS50 in the range of 400 ~ 4000 cm^{-1}.

Electrochemical measurement: Electrode preparation: catalyst powder (4 mg) was dispersed in a mixture of ultrapure water (350 μL), isopropanol (135 μL) and Nafion solution (20 μL; 5 wt%), and then the above-mentioned solution was ultrasonicated for 30 min to form a homogeneous ink. The obtained suspension solution (10 μL) was loaded onto a glassy carbon electrode surface (5 mm in diameter) to guarantee a uniform distribution. The commercial IrO_2 catalyst was used as a benchmark to assess the electrocatalytic performance of CoFe-PBA and CoFeZn-PBA.

Electrochemical characterization: the electrochemistry performances were tested on Zahner electrochemical workstation in a three-electrode configuration. The prepared electrode was used as the working electrode, while an Hg/HgO electrode (1.0 M KOH) and a carbon rod were used as the reference electrode and the counter electrode, respectively. The OER performances of working electrode were evaluated by linear sweep voltammetry (LSV) in 1.0 M KOH solution with the potential range of 0 ~ 1.5 V at a scan rate of 10 mV s^{-1}. The potentials were calibrated and transformed to the reversible hydrogen electrode (RHE) according to the following equation: $E_{(RHE)}$ =

$E_{(Hg/HgO)}$ + 0.059 × pH + 0.098 (pH = 14), and the overpotential (η) was calculated according to the equation of $\eta = E_{(RHE)} - 1.23$ V. Tafel plots (η versus log *j*, *j* is the current density) were directly obtained from the corresponding LSV curves. Cyclic voltammetry (CV) curves were measured in proper potential range of 1.25 ~ 1.35 V with different scanning rates of 10, 20, 30, 40, 50 and 60 mV s^{-1}. Electrochemical impedance spectroscopy (EIS) was performed in the frequency of 0.01 ~ 10^5 Hz at 5 mV. Stability test was conducted by chronoamperometry measurement. All the electrochemical data were presented without iR-compensation.

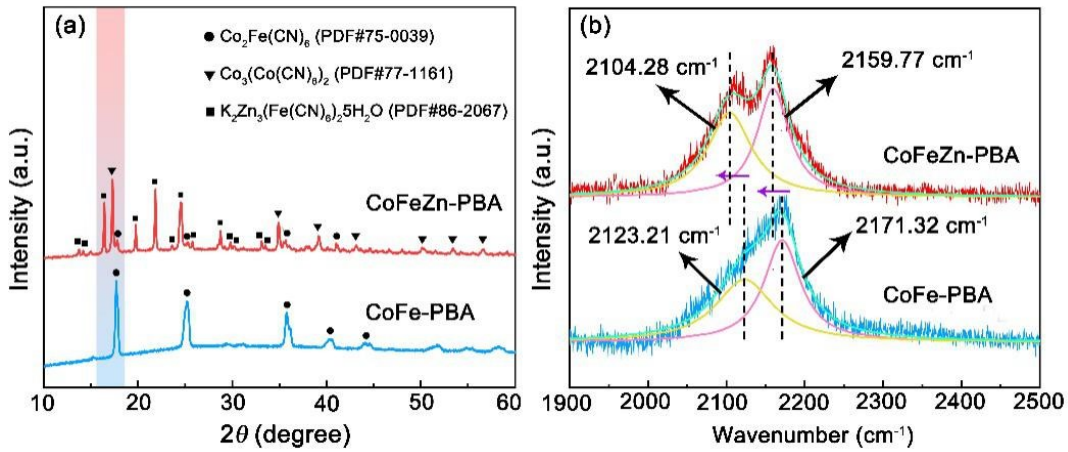

Fig. S1 (a) XRD patterns and (b) Raman spectra of CoFe-PBA and CoFeZn-PBA. The Raman shift is marked by purple arrows.

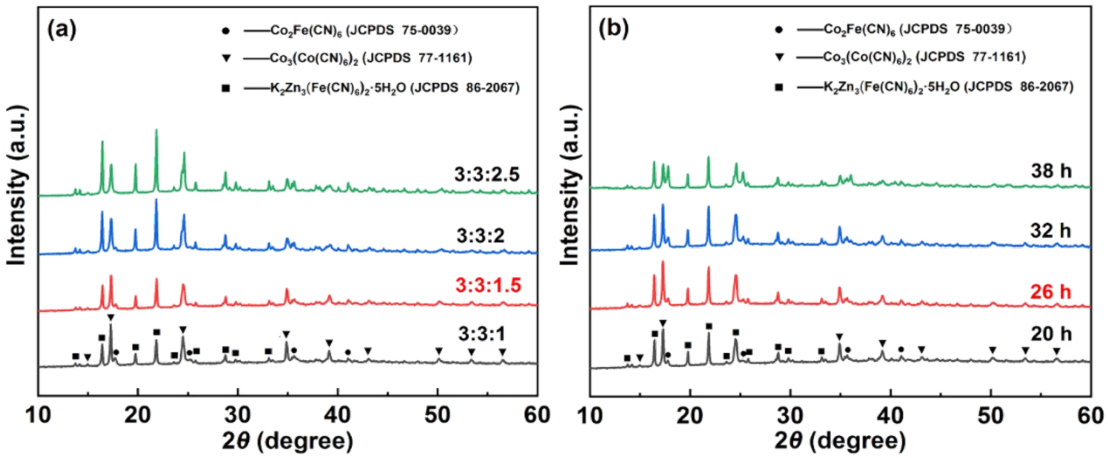

Fig. S2 XRD patterns of CoFeZn-PBA prepared with (a) different Zn^{2+} appending proportions, and (b) different co-precipitation times.

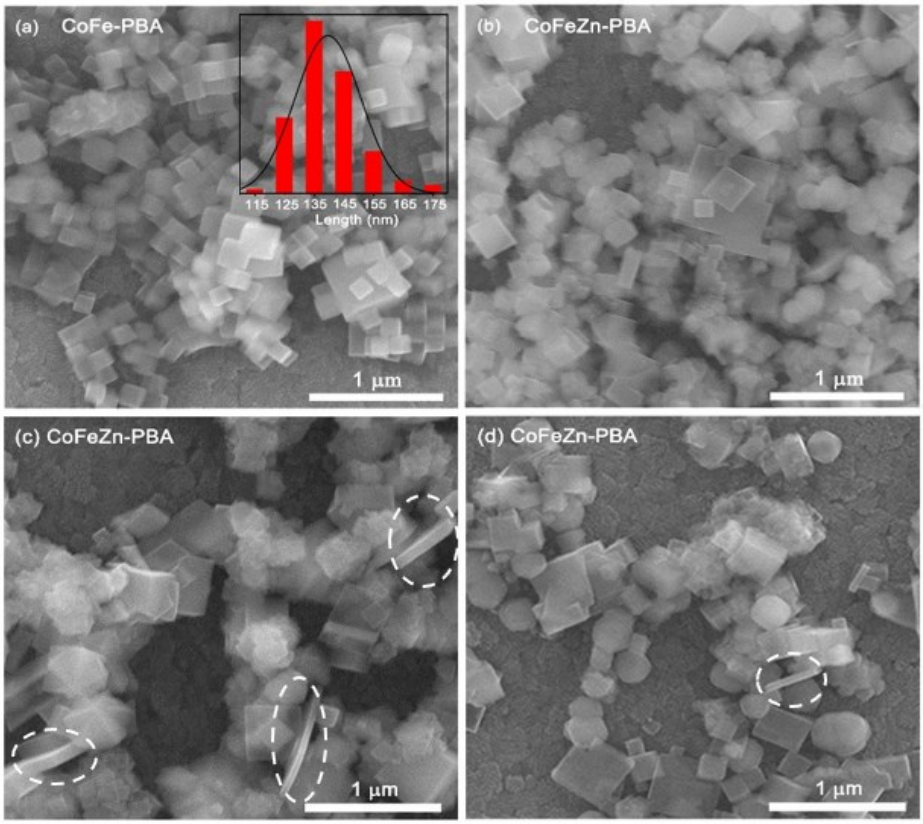

Fig. S3 (a) SEM image and nanocube size distribution of CoFe-PBA. (b), (c) and (d) SEM images of CoFeZn-PBA from different views. Nano-flakes are marked by white circles.

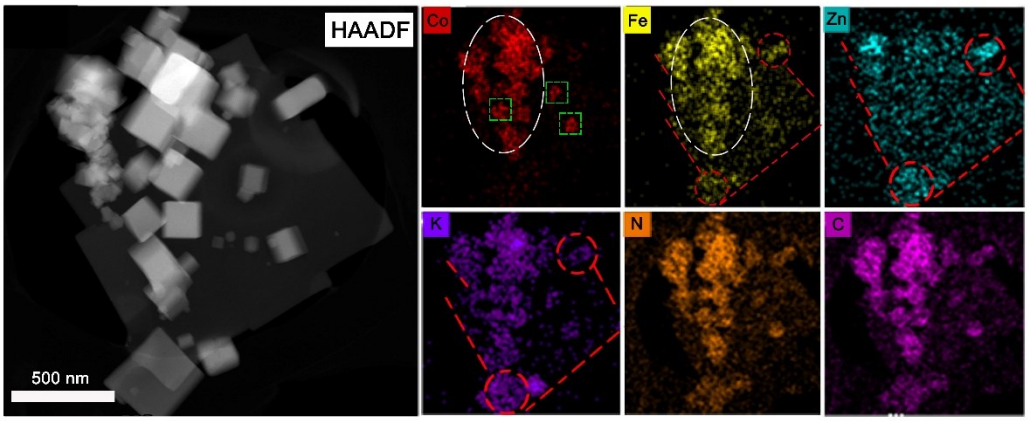

Fig. S4 HADDF-STEM image and EDX mapping of Co, Fe, Zn, K, C and N in the CoFeZn-PBA.

The elements are not evenly distributed: (1) The Co and Fe elements are clearly distributed in the position of the white area, which matches well with the position of nanocube and nanoparticle morphologies in the HADDF-STEM image, thus the nanocube and nanoparticle morphologies can be assigned to the mixture of $Co_2Fe(CN)_6$ and $Co_3[Co(CN)_6]_2$ in CoFeZn-PBA. The nanocube morphology is consistent with the SEM image of CoFe-PBA (Fig. S5a). The green box has only Co aggregation, which can attribute to the CoCo-PBA sample. (2) Clearly, the Zn element is mainly distributed in the position marked by red dotted line and red dotted circle. Moreover, the appearance of Zn element is always accompanied by the coexistence of Fe and K elements, and no distinct Co signals can be found in these regions. Such element distribution features match well with the position of the nanoflakes in the HADDF-STEM image. Thus, the nanoflakes can be assigned to $K_2Zn_3[Fe(CN)_6]_2 \cdot 5H_2O$. The N and C elements are clearly distributed throughout the whole testing range, and the different elements aggregation degree is mainly determined by different sample thickness and sample overlap degree.

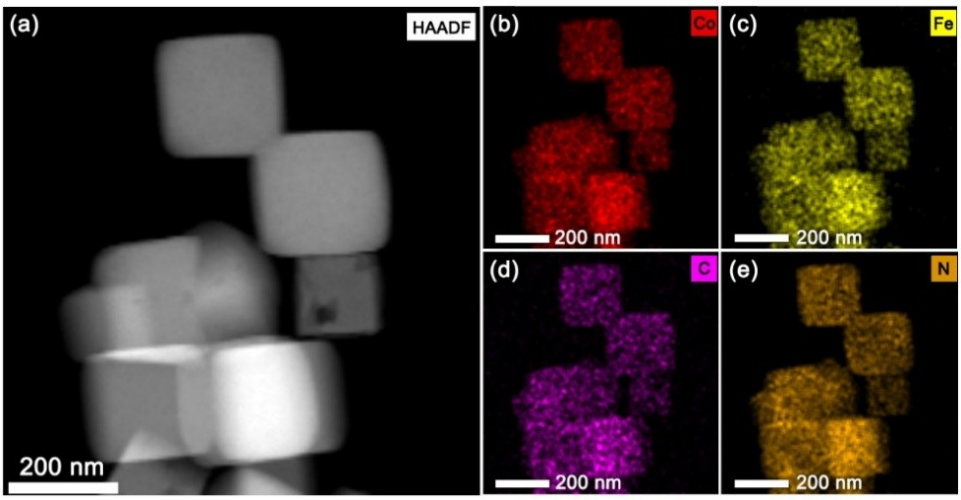

Fig. S5 (a) HADDF-STEM image of CoFe-PBA. EDX mapping of (b) Co, (c) Fe, (d) C, and (e) N in CoFe-PBA, respectively.

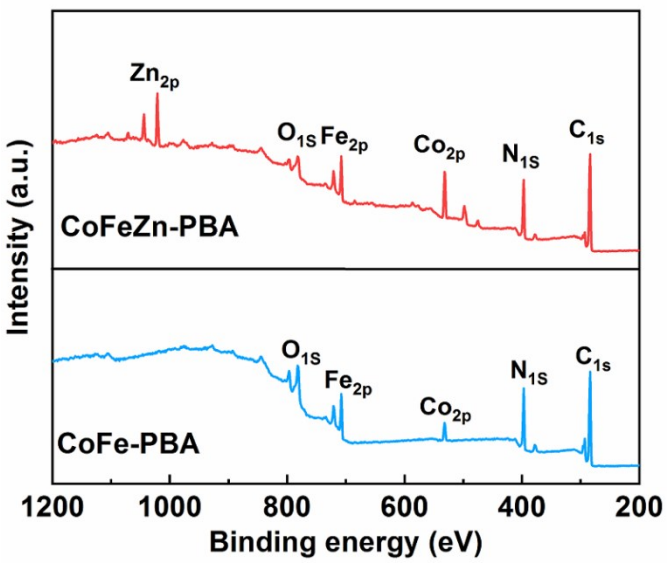

Fig. S6 XPS survey spectra of CoFeZn-PBA and CoFe-PBA.

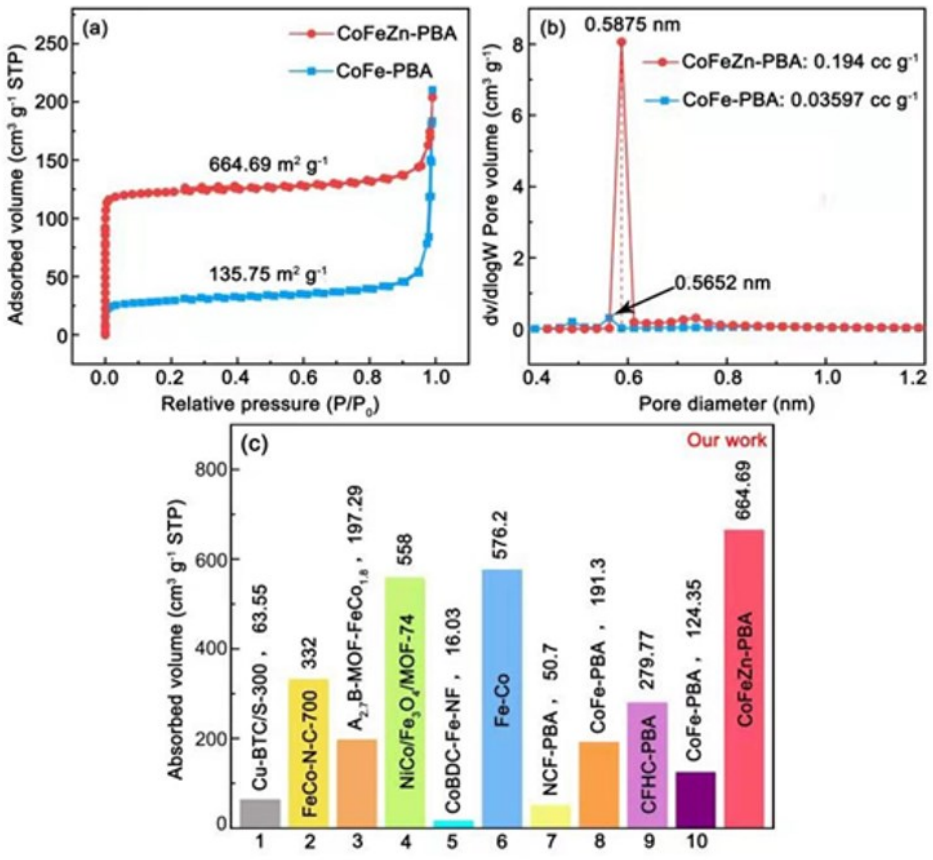

Fig. S7 (a) N_2 adsorption-desorption isotherm and (b) the corresponding pore size distribution plot of CoFeZn-PBA and CoFe-PBA samples. (c) Specific surface area values of several MOF electrocatalysts for OER.

As shown in Fig. S7a-b, both samples before and after Zn^{2+} incorporation exhibit a typical microporous structure with a pore size distribution ranging from 0.40 to 1.2 nm. Impressively, the CoFeZn-PBA sample shows a sharp peak at a pore diameter of 0.5875 nm, indicating a more uniform pore size. The pore volume of CoFeZn-PBA was calculated to be 0.194 cc g^{-1}, over 5 times as large as that of CoFe-PBA (0.036 cc g^{-1}).

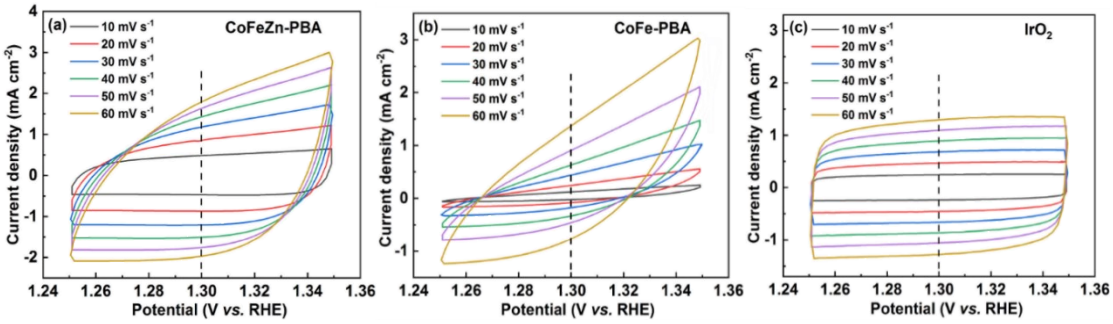

Fig. S8 Cyclicvoltammetry curves of (a) CoFeZn-PBA, (b) CoFe-PBA and (c) IrO_2 at potential window of 1.25-1.35V vs. RHE with different scanning rates of 10, 20, 30, 40, 50 and 60 mV s^{-1}.

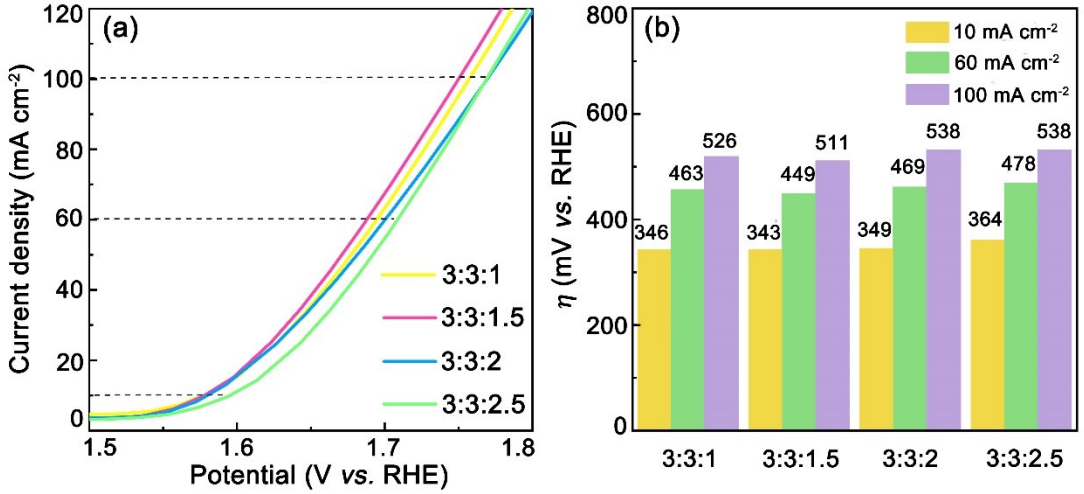

Fig. S9 (a) OER polarization curves of CoFeZn-PBA synthesized with different element proportion and (b) their corresponding overpotential required for j = 10, 60, and 100 mA cm^{-2}.

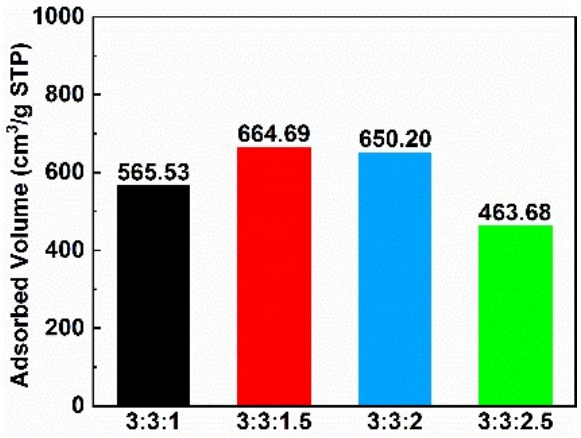

Fig. S10 Specific surface area values of CoFeZn-PBA with different Zn^{2+} appending proportions.

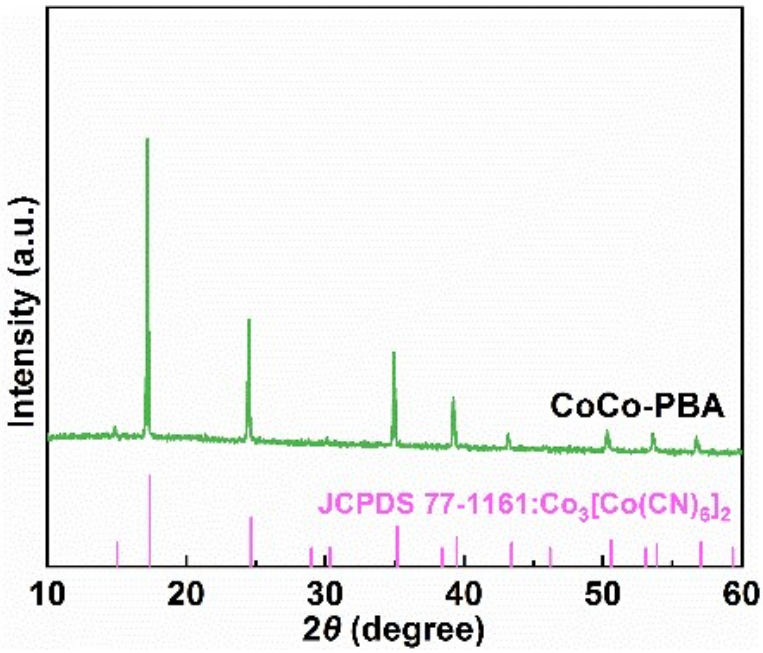

Fig. S11 XRD pattern of CoCo-PBA

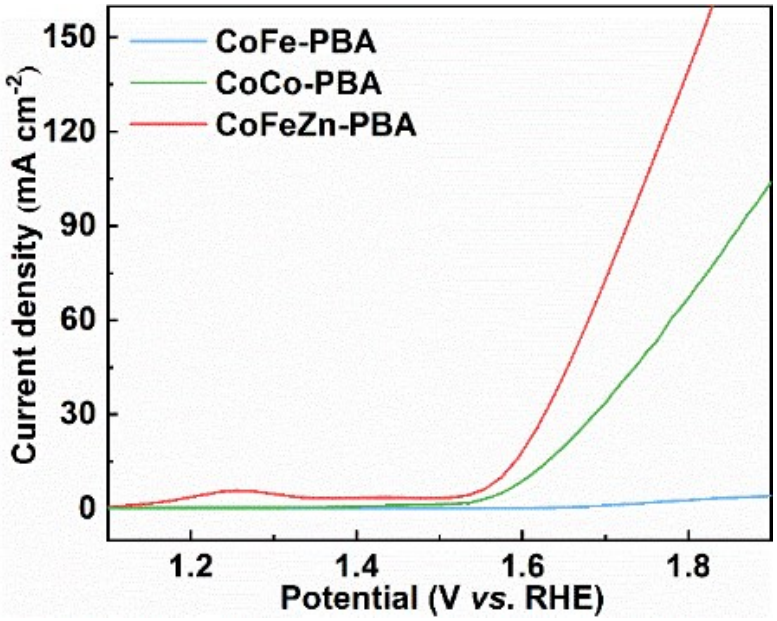

Fig. S12 OER polarization curves of CoFeZn-PBA, CoCo-PBAand CoFe-PBA .

On the one hand, even though the CoCo-PBA sample possesses a higher Co^{3+}/Co^{2+} ratio than CoFeZn-PBA (1.88 vs. 0.96) its specific surface area is much lower than that of CoFeZn-PBA (80.12 $m^2\ g^{-1}$ vs. 664.69 $m^2\ g^{-1}$), responsible for its lower activity. On the other hand, the specific surface area of CoCo-PBA is lower than that of CoFe-PBA, but the former exhibits a rather higher Co^{3+}/Co^{2+} ratio than the latter, indicating the critical role of high valance Co in OER. These results validate that the resultant higher Co^{3+}/Co^{2+} ratio and larger specific surface area upon Zn introduction are collectively accountable for outstanding OER performance in CoFeZn-PBA.

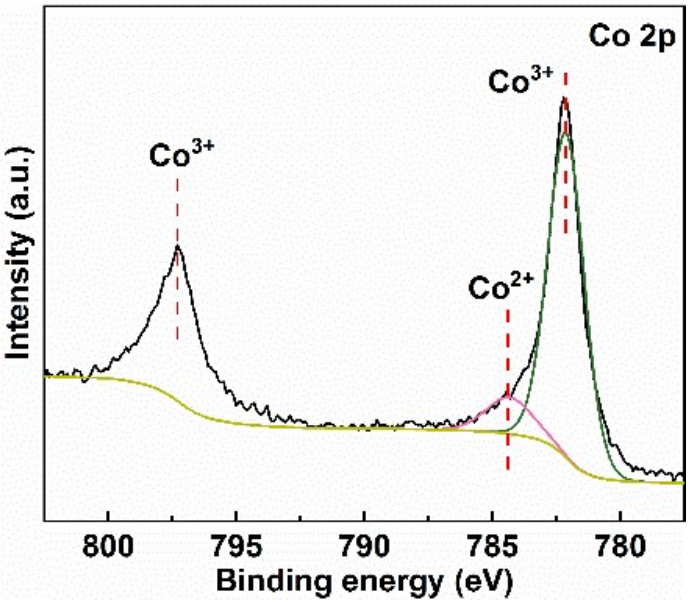

Fig. S13 High-resolution XPS spectrum of Co 2p for CoCo-PBA.

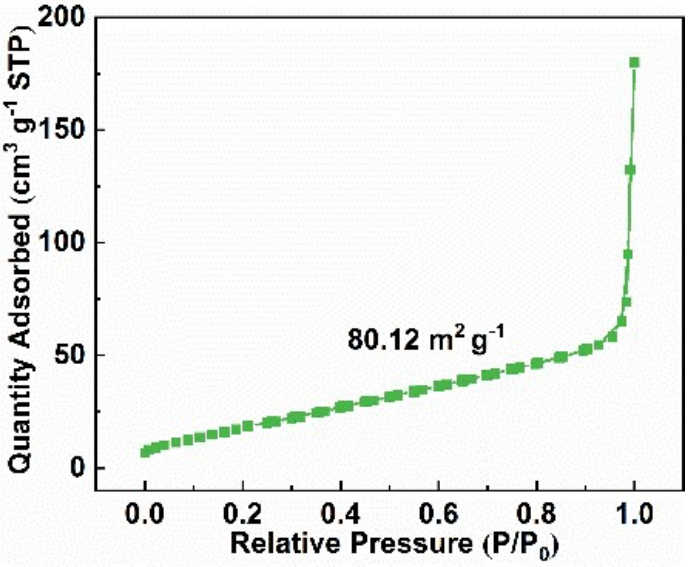

Fig. S14 N_2 adsorption/desorption isotherm for CoCo-PBA.

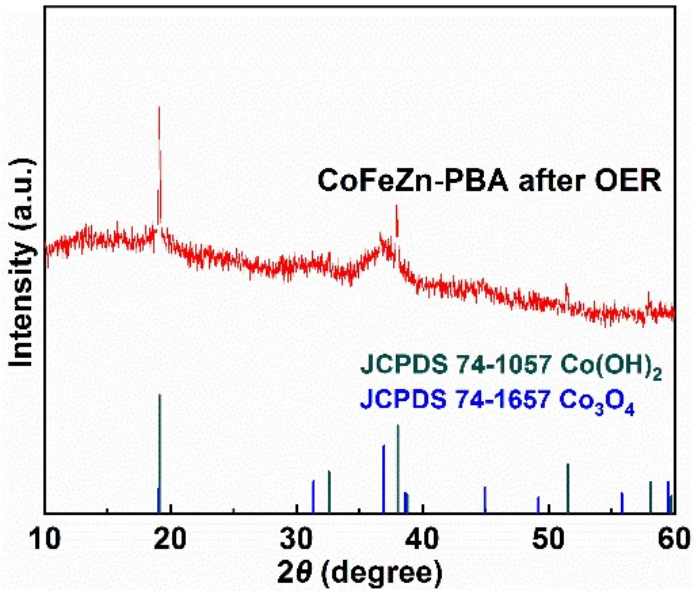

Fig. S15 XRD pattern of CoFeZn-PBA after OER.

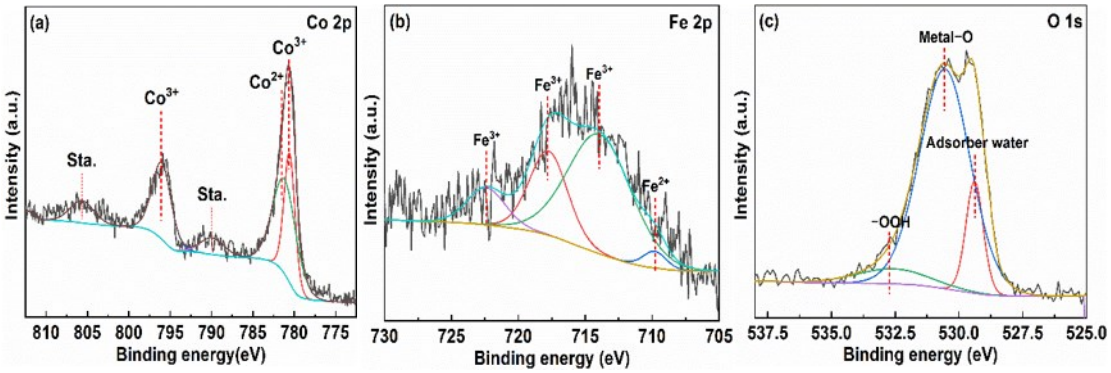

Fig. S16 High-resolution XPS of CoFeZn-PBA after OER (a) Co 2p spectrum, (b) Fe 2p spectrum and (c) O 1s spectrum.

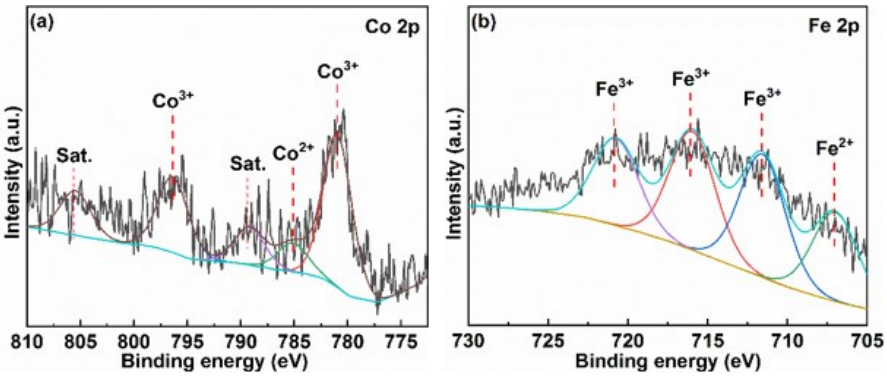

Fig. S17 High-resolution XPS of CoFe-PBA after OER (a) Co 2p spectrum and (b) Fe 2p spectrum.

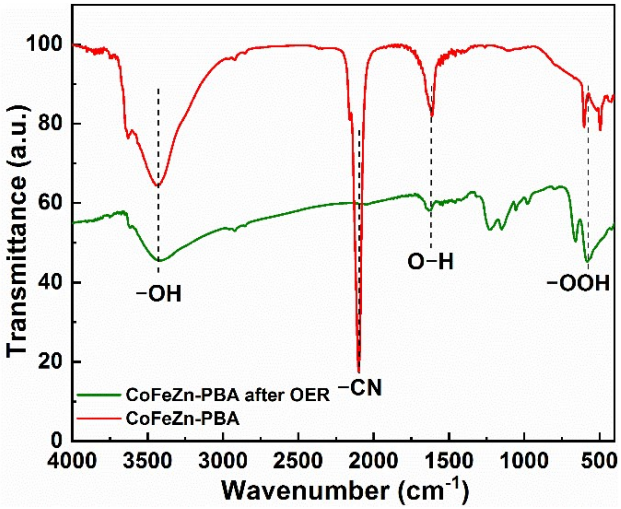

Fig. S18 Comparison of FTIR spectra of CoFeZn-PBA before and after OER.

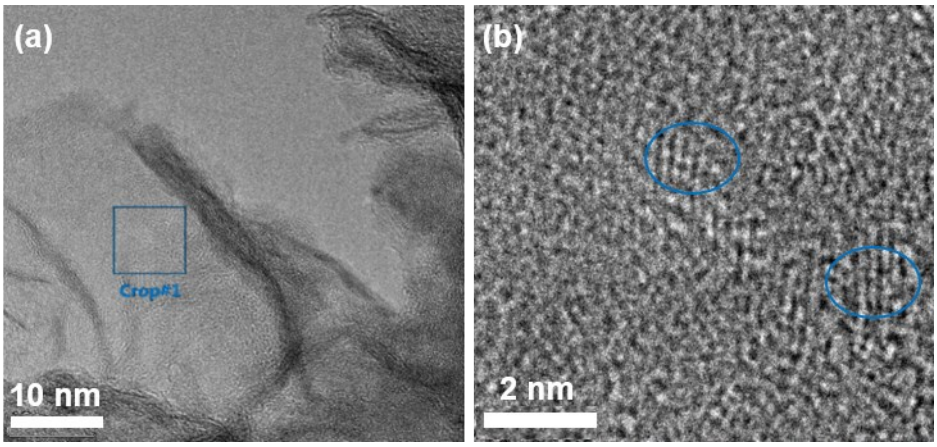

Fig. S19 TEM images of CoFeZn-PBA after OER.

Table S1. The OER properties of several representative transition-metal electrocatalysts.

	electrode	Overpotential (10 mV cm^{-2})	Overpotential (60 mV cm^{-2})	Overpotential (100 mV cm^{-2})	Tafel slope (mV dec^{-1})
FeCo PBA [1]	RDE	391	520	NULL	
FeCo PBA [2]	NF	356		450	84
O,N-NiFeCx-300 [3]	GCE	355	450	520	49
MnFe PBA [4]	GCE	632			55.69
CoFe@NC-NCNT-H [5]	GCE	379			99.6
FeCo-NCNFs[6]	GCE	456	1030		60
NiFe@NC [7]	GCE	360			81
FeCoNi alloys [8]	RDE	332	450		86
Co3ZnC/Co@CN [9]	GCDE	366	486		81
CoNiFe [10]	RDE	470			229
CoFeZn PBA (This work)	GCE	343	449	511	75

References

1. X. Ding, W. Uddin, H. T. Sheng, P. Li, Y. X. Du, M. Z. Zhu, *J. Alloy. Compd*, 2020, **814**, 152332.S.
2. T. I. Singh, G. Rajeshkhanna, S. B. Singh, T. Kshetri, N. H. Kim, J. H. Lee, *Chem. Sus. Chem*, 2019, **12**, 4810-4823.
3. B. He, P. Y. Kuang, X. H. Li, H. Chen, J. G. Yu, K. Fan, *Chem. Eur. J*, 2019, **25**, 1-12.
4. Y. Y. Wang, Y. Wang, L. Zhang, C. S. Liu, H. Pang, *Chem. Asian J*, 2019, **14**, 2790-2795.
5. Z. X. Shang, Z. L. Chen, Z. B. Zhang, J. Yu, S. Z. Tan, F. Ciucci, Z. P. Shao, H. Lei, D. J. Chen, *J. Alloy. Compd*, 2018, **740**, 743-753.
6. L. J. Yang, S. Z. Feng, G. C. Xu, B. Wei, L. Zhang, *ACS Sustainable Chem. Eng*, 2019, **7**, 5462-5475.
7. L. Du, L. L. Luo, Z. X. Feng, M. Engelhard, X. H. Xie, B. H. Han, J. M. Sun, J. H. Zhang, G. P. Yin, C. M. Wang, Yong Wang, Y. Y. Shao, *Nano Energy*, 2017, **39**, 245-252.
8. S. Gupta, L. Qiao, S. Zhao, H. Xu, Y. Lin, S. V. Devaguptapu, X. L. Wang, M. T. Swihart, G. Wu, *Adv. Energy Mater*, 2016, **6**, 1601198.
9. J. W. Su, G. L. Xia, R. Li, Y. Yang, J. T. Chen, R. H. Shi, P. Jiang, Q. W. Chen, *J. Mater. Chem. A*, 2016, **4**, 9204-9212.
10. J. Liu, S. T. Wei, N. B. Li, L. Zhang, X. Q. Cui, *Electrochimica Acta*, 2019, **299**, 575-581.